



Improved Creep and Tensile Properties of a Corrosion Resistant Ni-Based Superalloy Using High Temperature Aging and Nb/Ta Additions

MARTIN DETROIS, STOICHKO ANTONOV, KYLE A. ROZMAN, JEFFREY A. HAWK, and PAUL D. JABLONSKI

Resistance to creep deformation is essential for cast and wrought Ni-based superalloys in next generation energy systems due to the considerable exposure times required at the operating temperature. The amount of precipitate strengthening was increased in variants to Inconel alloy 725 (IN725), a corrosion resistant alloy, to improve its elevated temperature mechanical strength. Additions of Nb or Ta coupled with a high temperature aging (HTA) heat treatment promoted the formation of γ'' precipitates and grain boundary phases which led to significant increases in time to failure. The HTA increased the creep life of various alloy formulations as compared to the standard aging heat treatment with a maximum improvement of 371 pct. The Nb and Ta additions lowered the minimum creep rate (MCR) and had a similar effect on increasing creep life. The positive effect of the additions was more pronounced when coupled with the HTA which employed a higher temperature in the first step of the heat treatment to promote precipitate phase formation. The Ti/Al ratio was used to design alloys with preferential formation of γ' or γ'' precipitates. Compact morphology precipitates were formed in the alloys with a low Ti/Al ratio. While a low Ti/Al ratio was primarily associated with lower MCRs, the effect on the creep life was less evident than that of the HTA. Using additions of Nb or Ta and a HTA heat treatment, the creep life of IN725 for testing at 973 K (700 °C) and 483 MPa was improved by up to 256 pct.

<https://doi.org/10.1007/s11661-022-06690-6>

This is a U.S. government work and not under copyright protection in the U.S.; foreign copyright protection may apply 2022

I. INTRODUCTION

THE growing demand for clean energy alongside increasing electricity consumption is creating technical challenges for next generation energy systems. Higher efficiencies and lower emissions are needed. One approach to answer the stronger design requirements consists of increasing the operating temperature, such as in future advanced ultra-supercritical (AUSC) power plants^[1], thereby increasing efficiency and reducing harmful gas emissions. Further environmental concerns are addressed through carbon capture, utilization, and

sequestration (CCUS) processes. This approach targets operating temperatures above 973 K (700 °C), ≥ 50 K (50 °C) above current maximum temperatures.^[2] Alternatively, molten salt reactor or hydrogen turbines will require alloys with an exceptional combination of resistance to environmental degradation and deformation. Consequently, Ni-based superalloys have been investigated for use in the hot section of the power plant, such as in the steam turbine or boiler.^[3–6] Particularly, existing Ni-based superalloys, developed for use in land-based gas turbines or in commercial aircraft engines, are considered. This requires additional efforts to adapt them to the new environment which is associated with considerably longer exposure times at the operating temperature.^[7]

Inconel alloy 725, referred to as IN725, is a precipitate-strengthened Ni-based superalloy with high strength and corrosion resistance.^[8] The alloy is particularly attractive for use in corrosive environments due to its resistance to aqueous corrosion, pitting corrosion and stress corrosion cracking. It is a derivative of alloy 625 with added Ti to enable precipitate strengthening.^[9] The typical microstructure of IN725 consists of a

MARTIN DETROIS, STOICHKO ANTONOV, JEFFREY A. HAWK, and PAUL D. JABLONSKI are with the National Energy Technology Laboratory, 1450 Queen Ave. SW, Albany, OR, 97321. KYLE A. ROZMAN is with the National Energy Technology Laboratory and also with the NETL Support Contractor, 1450 Queen Ave. SW, Albany, OR, 97321. Contact e-mail: martin.detroit@netl.doe.gov.

Manuscript submitted November 29, 2021; accepted April 7, 2022.

Article published online April 28, 2022

face-centered cubic (FCC) γ matrix with γ'/γ'' precipitates embedded within. The γ' phase entails $\text{Ni}_3(\text{Al,Ti})$ with an ordered FCC L1_2 crystal structure, while the γ'' precipitates are typically Ni_3Nb with an ordered body-centered tetragonal (BCT) D0_{22} crystal structure. Carbides are also found in the alloy in the form of MC (Ti/Nb-rich), M_{23}C_6 (Cr-rich) and M_6C (Mo-rich). These carbides are primarily located along the grain boundaries (GBs).^[10] In addition, η phase has been reported to precipitate in IN725 when exposed to temperatures between 1023 K (750 °C) and 1173 K (900 °C), usually at exposure times above 10 and 100 hour, depending on the temperature.^[10,11] The η phase has an ordered hexagonal D0_{24} crystal structure and a typical composition consisting of Ni_3Ti . It forms in the shape of thin plates along, or originating from, the GBs.^[12]

In addition to its resistance to harsh environments, IN725 has good mechanical properties at low temperatures. In contrast to alloys 706 and 718, few investigations have been conducted on the performance of IN725 at elevated temperatures, such as in the 873 K (600 °C) to 1073 K (800 °C) range since the alloy was not originally designed for such environments.^[13] However, a recent investigation revealed potential for use of IN725 at elevated temperature when using Nb or Ta additions to increase the precipitation of phases of interest.^[14] These elements are prone to the formation of γ'' and/or δ phase which has a composition similar to γ'' but with a different crystal structure, namely D0_a . Small δ phase precipitates are formed for instance in Inconel alloy 718 (IN718) when using a high temperature aging heat treatment for the alloy.^[15,16] Similarly, small and stable η phase in alloy 718Plus have been shown to be beneficial to the mechanical properties, such as slowing fatigue crack growth rates.^[17] In this alloy, the composition of the η precipitates was identified as Ni_6AlNb as opposed to Ni_3Ti .^[18] Finally, coexistence of δ and η phase precipitates has been reported in several alloys.^[19,20]

The effect of Nb and Ta additions as well as varying the Ti/Al ratio was investigated with respect to microstructure and mechanical properties. Nb and Ta were considered for their influence on the GB phases, such as δ , and intragranular precipitates, such as γ'' . The Ti/Al ratio was considered to promote preferential precipitation of γ' or γ'' . In addition to the standard aging heat treatment formulated for IN725, an alternative, high temperature aging heat treatment, was designed to promote the formation of desirable precipitate phases. The influence of composition and microstructure on the mechanical properties of the alloys was assessed using creep and tension testing.

II. PROCEDURE

The alloys were developed from the starting composition for IN725, as described in Reference 8. A CALPHAD (CALculation of PHase Diagrams) approach was utilized to obtain the targeted compositions using Thermo-Calc with the TCNi8 database for

phase formation and JMatPro for kinetics. The baseline alloy, referred to as High(Ti/Al), consists of near nominal composition for IN725 with a Ti/Al ratio of 7.6. A variant, alloy Low(Ti/Al), with lower Ti and higher Al concentrations was considered with a Ti/Al ratio of 1.3. The amount of Nb + Ta was increased to 2.7 at. pct in the other alloys to promote the formation of GB phases, such as δ phase precipitates, according to plots from Reference 20 or γ'' precipitates within the matrix. Tantalum was added to alloys High(Ti/Al) and Low(Ti/Al) to form alloys Ta-High(Ti/Al) and Ta-Low(Ti/Al), respectively. Similarly, Nb was added to alloys High(Ti/Al) and Low(Ti/Al) to form alloys Nb-High(Ti/Al) and Nb-Low(Ti/Al), respectively.

High-purity, industry grade, stock materials were used to constitute the compositions of the alloys and form 8 kg ingots using vacuum induction melting. The charges were melted to a 50 K (50 °C) superheat temperature under 200 Torr Ar partial pressure. The liquid was poured into a 75 mm diameter cylindrical graphite mold with ceramic wash coat to prevent C pickup. Following solidification, approximately 5 mm thick slices were cut from the top of each ingot for chemistry analysis which is reported in Table I. Major constituting elements were determined using X-ray fluorescence (XRF) on a Rigaku ZSX Primus II while C, N, O and S were determined using combustion analysis on LECO systems. The tramp element concentrations are listed in Table II.

From Table I, the Ti/Al ratio was higher in alloys Ta-High(Ti/Al) and Nb-High(Ti/Al) compared to alloy High(Ti/Al) due to minor Al loss during melting of Ta-High(Ti/Al) and Nb-High(Ti/Al). Furthermore, the Nb + Ta concentration in atomic percent was slightly lower than the target of 2.7 in alloys Nb-High(Ti/Al) and Nb-Low(Ti/Al). This difference may not be accurate and could originate from the calibration of the XRF as it is unlikely to lose Nb during melting.

The ingots were homogenized in a vacuum heat treatment furnace under 50 Torr Ar partial pressure and using Ar forced gas fan cooling. The heat treatment schedule was optimized computationally for the alloys based on their chemistry and the ingot microstructure to reduce the predicted residual elemental inhomogeneity to below 1 pct.^[21] The heat treatment cycle consisted of 1303 K (1030 °C) for 1h, 1338 K (1065 °C) for 3h, 1363 K (1090 °C) for 3h, 1388 K (1115 °C) for 3h, 1408 K (1135 °C) for 6h and 1423 K (1150 °C) for 72h. Following homogenization, the ingot surfaces were finished on a lathe for hot working. Hot working consisted of steps of forging followed by steps of hot rolling with reheat between each pass to produce plates measuring 10 mm in thickness. The last reheat step was used as a solution heat treatment.

Two different aging heat treatments were investigated. The first consists of the standard aging heat treatment for IN725 and is referred to as standard aging (SA): 1003 K (730 °C) for 8h followed by cooling to 893 K (620 °C) at 1 K/min (1 °C/min) and holding at 893 K (620 °C) for 8h. The second aging heat treatment was designed to promote the formation of precipitate phases at higher temperatures, and thereby, is referred to as

Table I. Composition of the Alloys From XRF (Major Elements), Combustion Analysis (C) and Measured From Addition to the Melt (B) in Wt Pct Unless Otherwise Specified. Ni Balanced

Alloy	Cr	Mo	Ti	Al	Nb	Ta	Fe	Mn	Si	C	B	Ti/Al	Nb + Ta (At. Pct)
High(Ti/Al)	21.2	7.1	1.82	0.24	3.4	0.2	3.9	0.04	0.02	0.039	0.003	7.6	1.81
Ta-High(Ti/Al)	20.5	7.0	1.87	0.20	3.4	3.6	3.8	0.05	<0.01	0.049	0.003	9.4	2.69
Nb-High(Ti/Al)	20.6	7.1	1.88	0.19	4.6	0.4	3.9	0.05	<0.01	0.049	0.003	9.9	2.43
Low(Ti/Al)	21.2	7.1	1.10	0.85	3.4	0.4	3.9	0.06	0.03	0.044	0.003	1.3	1.90
Ta-Low(Ti/Al)	21.2	7.0	1.15	0.89	3.4	3.5	3.9	0.04	0.02	0.038	0.003	1.3	2.77
Nb-Low(Ti/Al)	21.3	7.1	1.13	0.84	4.5	0.4	3.9	0.04	0.01	0.040	0.003	1.3	2.50

Table II. Tramp Element Concentration in the Ingots From Combustion Analysis, in PPM

Alloy	N	O	S
High(Ti/Al)	17 ± 1	12 ± 1	9 ± 1
Ta-High(Ti/Al)	6 ± 2	37 ± 13	6 ± 3
Nb-High(Ti/Al)	8 ± 4	21 ± 1	2 ± 1
Low(Ti/Al)	17 ± 4	20 ± 1	9 ± 5
Ta-Low(Ti/Al)	6 ± 2	8 ± 1	6 ± 2
Nb-Low(Ti/Al)	11 ± 7	9 ± 1	6 ± 2

high temperature aging (HTA), described as follows: 1073 K (800 °C) for 20h followed by cooling to 1023 K (750 °C) at 1 K/min (1 °C/min) and holding at 1023 K (750 °C) for 8h. The aging heat treatments were performed in the vacuum heat treatment furnace under 50 Torr Ar partial pressure and Ar forced gas fan cooling was performed at the end of the cycles. Specimens characterized and mechanically tested received either the SA or HTA heat treatments.

Assessment of the mechanical performance of the alloys was performed in tension and creep. Test specimens consisted of reduced gage cylindrical samples of 76 mm in overall length and 10 mm in overall diameter with ANSI 3/8 × 16 threaded ends. The reduced gage section measured 32 mm in length and 6.3 mm in diameter. Tension testing was performed at room temperature (RT) and 1023 K (750 °C) according to ASTM E8 standard.^[22] Creep screening was performed according to ASTM E139 standard using a dead weight creep frame.^[23] Two conditions were selected for creep testing: 973 K (700 °C)/483 MPa and 1063 K (790 °C)/207 MPa. Calculation of minimum creep rate (MCR) was performed by an algorithm which both averaged the data set to get time and strain and performed a linear regression to get the strain rate; details can be found in Reference [24].

Observation of the microstructures was performed after standard metallographic sample preparation down to 0.05 μm using colloidal silica. The starting microstructures, *i.e.*, following aging and prior to deformation, were obtained from the threaded section of cross-sectioned tensile specimens tested at RT. Cross-sectioned crept specimens were also included for microstructural characterization. Observation of the

microstructure was performed on a FEI Inspect F scanning electron microscope (SEM) in backscatter electron mode and equipped with an Oxford Instrument X-Max energy dispersive spectrometer (EDS) for phase characterization.

Transmission electron microscopy (TEM) samples were prepared by extracting Ø3mm discs from the grip sections of the post-creep specimens. Following grinding on progressive grit papers to ~70μm, the TEM blanks were thinned to electron transparency using twin-jet polishing in a solution of 10 pct perchloric acid and 90 pct ethanol at -20 °C and 21 V. A JEOL JEM 2100PLUS, operating at 200 kV, was used for selected area diffraction (SAD) and bright field (BF) and dark-field (DF) imaging.

III. RESULTS

A. Computational Work

The predictions from Thermo-Calc are shown in Figure 1 for the six alloys from 873 K (600 °C) to 1673 K (1400 °C) and from 0.001 to 1 mole fraction of all phases. From Figure 1(a) and (d), the modification to the Ti and Al contents are predicted to decrease the amount and solvus temperature of δ phase and slightly increase the amount of γ'. In alloy Low(Ti/Al), η phase is predicted to form at temperatures up to 923 K (650 °C). The increase in the Nb + Ta content in the other alloys resulted in improved stability of the δ phase with similar amounts in alloys Ta-High(Ti/Al) and Nb-High(Ti/Al), and Ta-Low(Ti/Al) and Nb-Low(Ti/Al), as shown in Figures 1(b), (c), (e) and (f), respectively. This occurred at the expense of the γ' phase with lower fractions and solvus temperatures, particularly in alloys Ta-High(Ti/Al), Nb-High(Ti/Al) and Ta-Low(Ti/Al). In alloy Ta-High(Ti/Al), Figure 1(b), the γ' phase was not predicted to form in the temperature and mole fraction range considered. Finally, η phase was significantly more stable in the high-Ta alloys Ta-High(Ti/Al) and Ta-Low(Ti/Al), Figure 1(b) and e, with amounts and solvus temperatures similar to the γ' phase in the respective baseline alloys High(Ti/Al) and Low(Ti/Al), Figures 1(a) and (d). The η phase is predicted to coexist with γ' in alloy Ta-Low(Ti/Al), Figure 1(e).

It is important to note the “NI3TA_D022” phase, known as γ'', was selected in Thermo-Calc, however, it

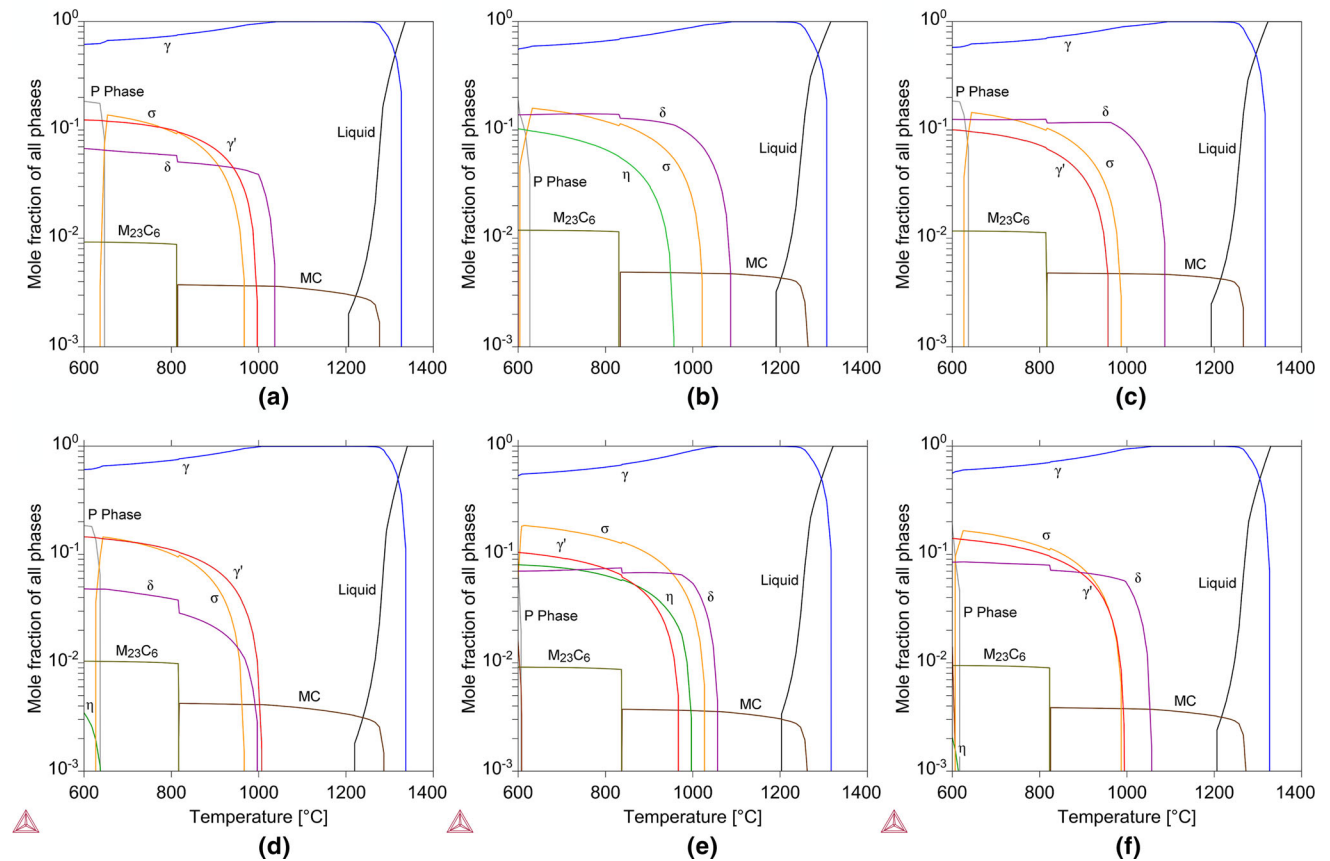


Fig. 1—Thermo-Calc predictions for alloys (a) High(Ti/Al), (b) Ta-High(Ti/Al), (c) Nb-High(Ti/Al), (d) Low(Ti/Al), (e) Ta-Low(Ti/Al) and (f) Nb-Low(Ti/Al) using the TCNi8 database.

was not predicted to form. Instead, δ , as shown in Figure 1 and labelled “NI3TA_D0A” in Thermo-Calc, was predicted to be stable.

The compositions of the precipitate phases γ' , δ , η and σ in each alloy at 973 K (700 °C) and as predicted from the Thermo-Calc simulations are listed in Table III. The γ' phase is predicted to be $\text{Ni}_3(\text{Ti}, \text{Al}, \text{Nb})$. The precipitates in the high Ti/Al ratio alloys High(Ti/Al) and Nb-High(Ti/Al) were rich in Ti and lean in Al with an approximated composition of $\text{Ni}_3\text{Ti}_{0.6}\text{Al}_{0.1}\text{Nb}_{0.3}$. The precipitates in the low Ti/Al ratio alloys Low(Ti/Al), Ta-Low(Ti/Al) and Nb-Low(Ti/Al) are predicted to have almost equimolar concentrations of Ti, Al and Nb resulting in the approximated composition of $\text{Ni}_3\text{Ti}_{0.33}\text{Al}_{0.33}\text{Nb}_{0.33}$. The δ phase precipitates are predicted to be $\text{Ni}_3(\text{Nb}, \text{Ti})$ and are Nb-rich over Ti. Decreasing the Ti/Al ratio is predicted to slightly increase the Nb and decrease the Ti concentrations in the precipitates. Furthermore, slight partitioning of Ta over 1 at. pct was predicted in the high-Ta alloys Ta-High(Ti/Al) and Ta-Low(Ti/Al). In those alloys, the η phase precipitates had strong differences in composition. While the composition was $\text{Ni}_3(\text{Ti}, \text{Ta}, \text{Al})$, the Ti content was higher than that of Ta in the high Ti/Al ratio alloy Ta-High(Ti/Al) and lower than that of Al and Ta in the low Ti/Al ratio alloy Ta-Low(Ti/Al). In the latter, the precipitates are predicted to be rich in Ta

and Al. Finally, the composition of the σ phase was similar for all alloys and rich in Cr, Ni and Mo.

B. Microstructure

Images taken along the GBs of the as-aged alloys following the HTA heat treatment are shown in Figure 2. Two GBs are shown for each alloy to illustrate the degree of inhomogeneity with regards to the various precipitate phases that formed. Overall, different types of precipitates formed for each alloy. EDS analysis was performed on specimens exposed to 1033 K (760 °C) for 1,000 hour to allow growth of the precipitate and tentatively identify the various phases. Small blocky precipitates, which appear black or dark in all alloys, corroborated with M_{23}C_6 carbides with M being primarily Cr, at ~62 at. pct, followed by Mo and Ni depending on the alloy. The small blocky white precipitates are likely M_6C carbides from the high concentration of Mo with traces of Si.^[25] This correlates with other investigations on IN725.^[10] Finally, discrete needle/rod shaped precipitates were found in the alloys. These precipitates are consistent with δ and/or η phase with a primarily $\text{Ni}_3(\text{Nb}, \text{Ti})$ composition. The balance in the Nb, Ti concentration was generally different between the alloys with low and high Ti/Al ratio. The

Table III. Predicted Composition of Selected Phases for Major Elements, *i.e.*, <1 at. Pct is Omitted, at 973 K (700 °C) Using the TCNi8 Database (at. Pct).

Alloy	Phase	Ni	Cr	Mo	Ti	Al	Nb	Ta	Fe
High(Ti/Al)	γ'	75	—	—	13	3	8	—	—
	δ	75	—	—	7	—	17	—	—
	σ	31	40	27	—	—	—	—	3
Ta-High(Ti/Al)	δ	75	—	—	7	—	15	3	—
	η	75	—	—	13	4	—	8	—
Nb-High(Ti/Al)	γ'	75	—	—	14	3	8	—	—
	δ	75	—	—	7	—	17	—	—
Low(Ti/Al)	γ'	75	—	—	8	8	8	—	—
	δ	75	—	—	5	—	19	—	—
Ta-Low(Ti/Al)	γ'	75	—	—	9	8	8	—	—
	δ	75	—	—	5	—	18	1	—
	η	75	—	—	2	10	—	13	—
Nb-Low(Ti/Al)	γ'	75	—	—	8	9	8	—	—
	δ	75	—	—	4	—	19	—	—

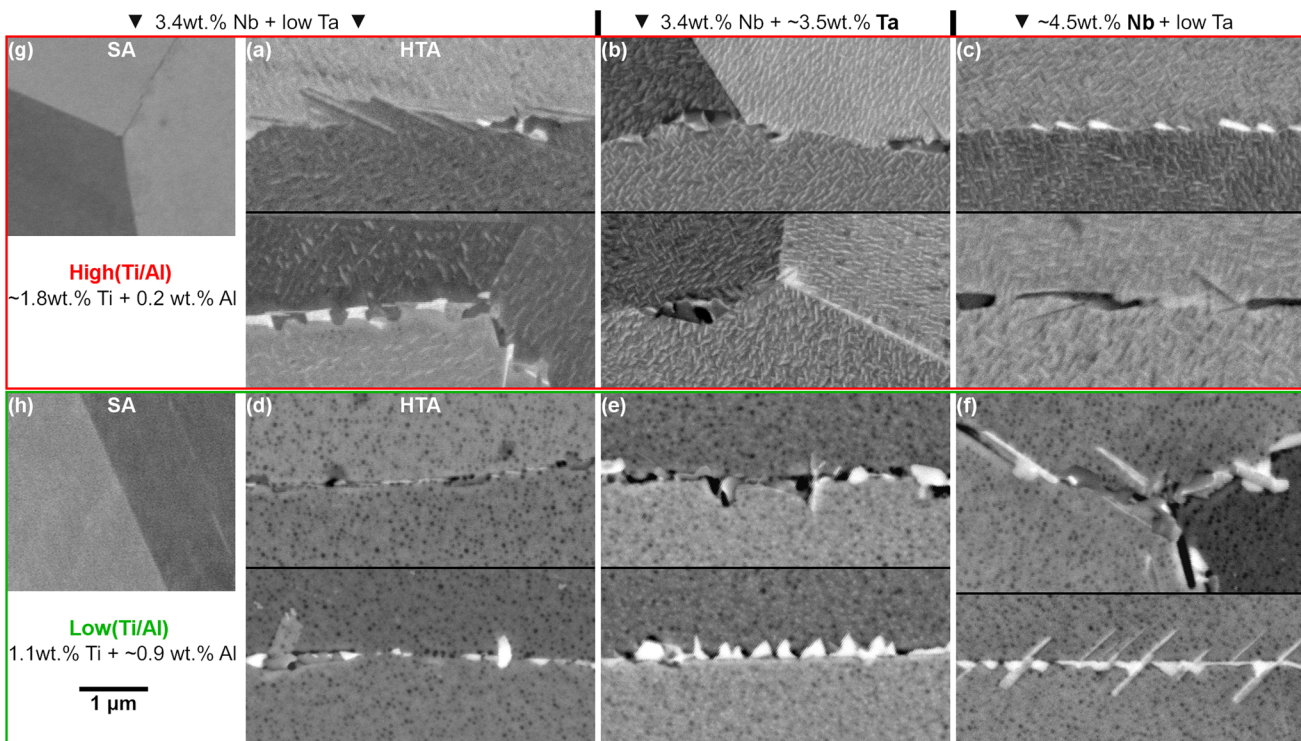


Fig. 2—SEM images of the GBs in the alloys (two locations were selected to illustrate the degree of inhomogeneity) following (a to f) the HTA heat treatment for alloys (a) High(Ti/Al), (b) Ta-High(Ti/Al), (c) Nb-High(Ti/Al), (d) Low(Ti/Al), (e) Ta-Low(Ti/Al) and (f) Nb-Low(Ti/Al) and for alloys (g) High(Ti/Al) and (h) Low(Ti/Al) with the SA heat treatment.

precipitates in the high Ti/Al ratio alloys tended to be richer in Ti than Nb while the opposite was found in the low Ti/Al alloys. Grain boundary precipitates were barely resolved on the SEM for the baseline alloy High(Ti/Al) and alloy Low(Ti/Al) with the SA heat treatment, Figure 2(g) and (h), respectively.

The microstructure of the alloys in the bulk of the grains are shown in Figure 3 as TEM-BF images from the $[001]_{\gamma}$ zone axis. The images were obtained on specimens tested in creep at 973 K (700 °C) and 483 MPa from the grip sections (no effect of strain). For the

specimens having received the HTA heat treatment, Figures 3(a) through (f), formation of γ' and γ'' precipitates were found for all alloys, with the exception of alloy Nb-High(Ti/Al), Figure 3(c), which precipitated γ'' but not γ' . Overall, the alloys with a high Ti/Al ratio showed preferred precipitation of γ'' precipitates as opposed to γ' , see Figures 3(a) through (c). On the other hand, increasing the Al content and decreasing Ti was favorable for the formation of γ' precipitates, Figures 3(d) through (f). Compact precipitates formed

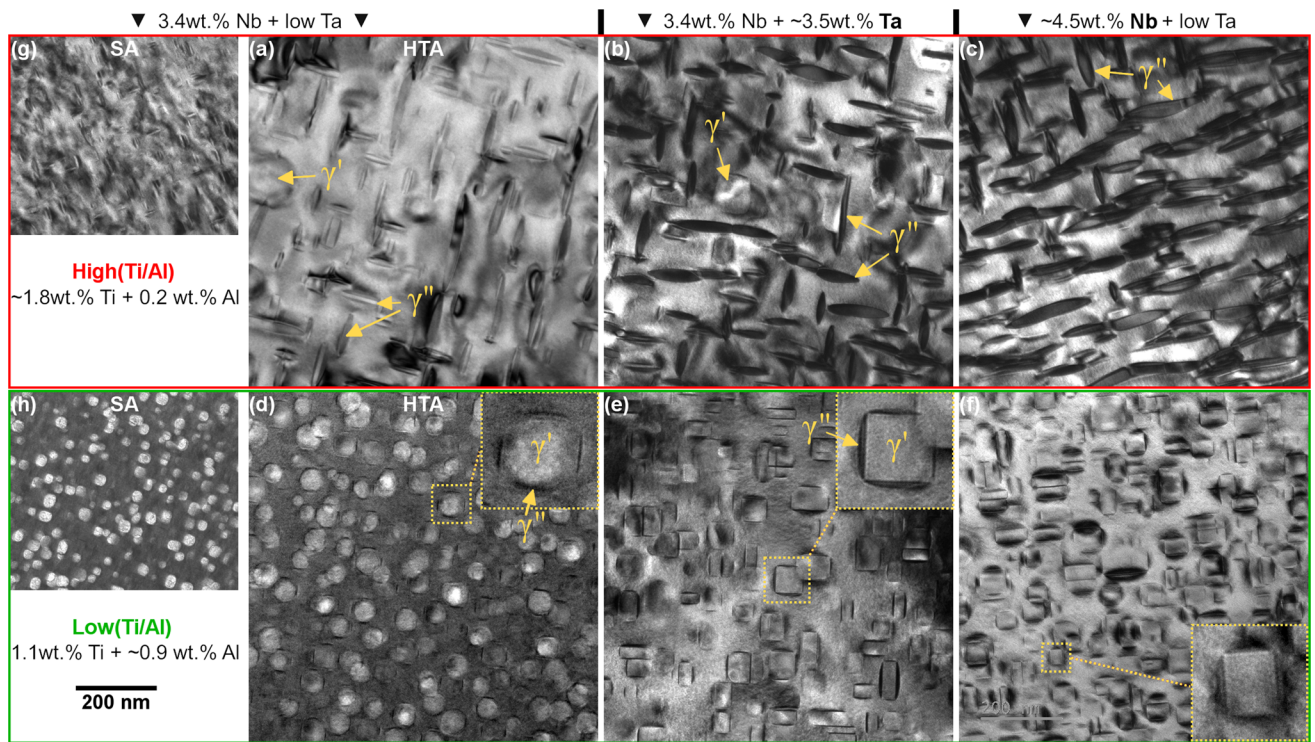


Fig. 3—TEM-BF images of the intragranular microstructure of the alloys from the grip sections of the specimens tested in creep at 973 K (700 °C) and 483 MPa showing the γ' and γ'' precipitates following (a to f) the HTA heat treatment for alloys (a) High(Ti/Al), (b) Ta-High(Ti/Al), (c) Nb-High(Ti/Al), (d) Low(Ti/Al), (e) Ta-Low(Ti/Al) and (f) Nb-Low(Ti/Al) and for alloys (g) High(Ti/Al) and (h) Low(Ti/Al) with the SA heat treatment.

in the low Ti/Al ratio alloys which consisted of cuboidal γ' particles surrounded by γ'' precipitates forming a shell on the faces of the γ' precipitates. Compact precipitates have been reported in IN718^[26–28] and the design leading to their formation is the subject of a future investigation. Increasing the Nb and Ta content in alloys Nb-Low(Ti/Al), Figure 3(e), and Ta-Low(Ti/Al), Figure 3(f), reinforced the cuboidal morphology of the γ' precipitates and promoted the precipitation of γ'' precipitates which led to fully enclosed γ' precipitates in those alloys compared to Low(Ti/Al), as shown in Figure 3(d). In the high Ti/Al alloys, increasing the Nb and Ta content led to a denser repartition of the γ'' precipitates and destabilization of γ' . The specimens following the SA heat treatment contained smaller precipitates as compared to their counterparts that received the HTA heat treatment [Figures 3(g) vs 3(a) and Figures 3(h) vs 3(d)]. The microstructure contained γ'/γ'' precipitates for alloy High(Ti/Al), with a visually higher density of γ'' precipitates, and only γ' for alloy Low(Ti/Al). SAD patterns and DF images are provided in the supplementary material to underline these observations.

The grain size was calculated using the linear intersect technique for each alloy.^[29] Four regions were considered, each used to perform four measurements. The values are listed in Table IV and consist of the average grain size with standard deviations obtained between each region. The results revealed very similar grain sizes between the alloys at around 46–47 μm with the

exception of alloy Low(Ti/Al) which showed a slightly smaller grain size of 42 μm .

C. Creep

Results from creep screening are shown in Figure 4 in the form of elongation to failure as a function of creep life for the testing conditions 973 K (700 °C)/483 MPa, Figure 4(a), and 1063 K (790 °C)/207 MPa, Figure 4(b). Starting with the tests performed at 973 K (700 °C) and 483 MPa, Figure 4(a), the standard alloy High(Ti/Al) in the SA condition lasted 194 hour and showed a 9 pct elongation to failure. The HTA heat treatment showed improved time and elongation to failure with values equal to 271 hour and 14 pct, respectively. This observation is true for all alloys tested under the two different aging conditions. Note: Alloys Ta-High(Ti/Al) and Nb-High(Ti/Al) were only tested following the HTA heat treatment. Alloys Low(Ti/Al), Ta-Low(Ti/Al) and Nb-Low(Ti/Al) in the SA condition had the shortest lives (80, 104 and 171 hour, respectively) and the lowest elongations to failure (~1–2 pct). Significantly higher values were measured for those alloys following the HTA heat treatment with creep lives of 231, 490 and 432 hour and elongations to failure of 6, 4 and 5 pct, respectively. Alloys Ta-Low(Ti/Al), Nb-Low(Ti/Al), Ta-High(Ti/Al) and Nb-High(Ti/Al) in the HTA condition had the longest creep lives, greater than 400 hour, with a maximum of 690 hour for alloy Ta-High(Ti/Al).

Table IV. Grain Sizes for the Alloys Obtained Using the Linear Intersect Technique

Alloy	Grain Size (μm)
High(Ti/Al)	47 ± 3
Ta-High(Ti/Al)	46 ± 4
Nb-High(Ti/Al)	46 ± 4
Low(Ti/Al)	42 ± 2
Ta-Low(Ti/Al)	47 ± 2
Nb-Low(Ti/Al)	47 ± 3

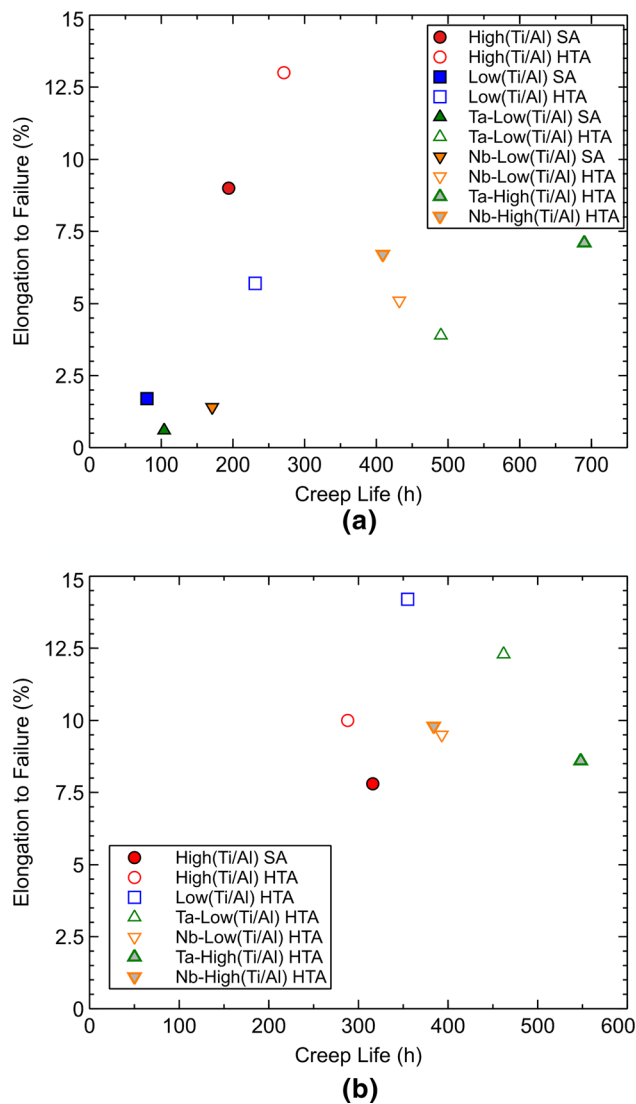


Fig. 4—Elongation to failure as a function of creep life at (a) 973 K (700 °C) and 483 MPa and (b) 1063 K (790 °C) and 207 MPa for the alloys after SA or HTA heat treatment.

Observation of the fracture surfaces revealed a mixed intergranular/transgranular failure with predominant intergranular mode for all specimens tested under those conditions, as shown in Figure 5. Overall, the HTA resulted in a more ductile failure as shown in Figure 5(b) for alloy High(Ti/Al) where ductile shearing was more

abundant as compared to the SA condition, Figure 5(a). Alloys Ta-Low(Ti/Al) and Nb-Low(Ti/Al) following the HTA, Figures 5(c) and (d), respectively, presented fracture surfaces comparable to that of alloy High(Ti/Al) in the SA condition. Furthermore, less evidence of ductility, characterized by lack of evidence for shearing failure on the fracture surfaces, was found for alloy Ta-Low(Ti/Al) compared to alloy Nb-Low(Ti/Al).

Testing at higher temperature and lower stress, *i.e.*, 1063 K (790 °C) and 207 MPa, overall resulted in slightly improved times to failure, Figure 4(b). Alloys Ta-Low(Ti/Al), Nb-Low(Ti/Al), Ta-High(Ti/Al) and Nb-High(Ti/Al) in the HTA condition remained the best performing alloys in terms of creep life ranging from 384 to 548 hour. The elongation to failure for those ranged from 9 to 12 pct. Reductions in the elongation to failure were observed compared to the previous condition for alloy High(Ti/Al) following both aging conditions. Finally, alloy Low(Ti/Al) in the HTA condition presented the highest elongation to failure of 14 pct. Observation of the fracture surfaces following testing at 1063 K (790 °C) and 207 MPa revealed mixed intergranular/transgranular failure heavily biased towards intergranular failure with a significantly greater density of rupture dimples.

Microstructure images following creep testing at 973 K (700 °C) and 483 MPa were taken in the gauge section of the specimens, below the fracture surface. For all alloys, a denser repartition of precipitates was observed following creep testing when compared to the starting conditions, *i.e.*, following aging and prior to mechanical testing. This was more evident for alloys Nb-Low(Ti/Al) and Nb-High(Ti/Al). Example images are shown in Figure 6 for alloy High(Ti/Al), Figure 6(a), and alloy Nb-High(Ti/Al), Figure 6(b), in the as-aged condition (following the HTA heat treatment) compared to the crept specimens tested at 973 K (700 °C) and 483 MPa observed below the fracture surface.

D. Tension

Tension testing results are shown in Figure 7 for testing at room temperature (RT) and 1023 K (750 °C). Similar to the creep data, the alloys tested were High(Ti/Al), Low(Ti/Al), Ta-Low(Ti/Al) and Nb-Low(Ti/Al) with the SA and HTA heat treatments and Ta-High(Ti/Al) and Nb-High(Ti/Al) in the HTA condition. At RT, Figures 7(a) through (c), alloys Ta-High(Ti/Al) and Nb-High(Ti/Al) showed the greatest ultimate tensile strength (UTS) and 0.2 pct yield stress (YS) compared to the other alloys with values above 1350 MPa and 1000 MPa, respectively. The other alloys presented UTS values between 1169 and 1253 MPa with minor variations between SA and HTA heat treatments, see Figure 7(a). Generally, the YS of alloys High(Ti/Al) and Low(Ti/Al) were the lowest with values between 722 and 812 MPa, Figure 7(b). The YS was slightly higher for alloys Ta-Low(Ti/Al) and Nb-Low(Ti/Al) with values between 795 and 898 MPa. The highest elongation to failure were obtained for the alloys in the SA condition with values between 43 and 48 pct, as shown in Figure 7(c). Lower values were obtained in the alloy

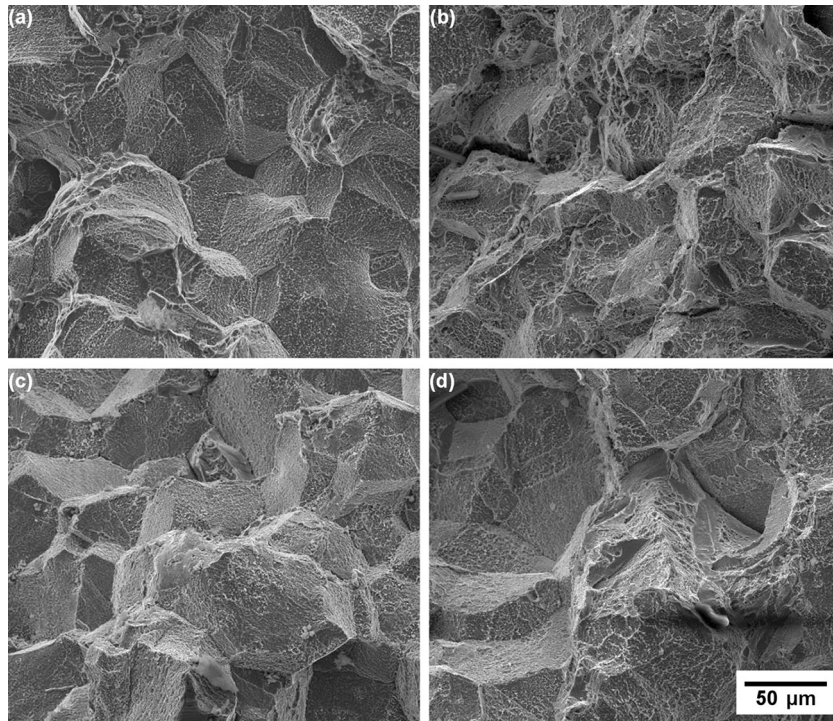


Fig. 5—Fracture surfaces following creep testing at 973 K (700 °C) and 483 MPa for the specimens (a) High(Ti/Al) SA, (b) High(Ti/Al) HTA, (c) Ta-Low(Ti/Al) HTA and (d) Nb-Low(Ti/Al) HTA.

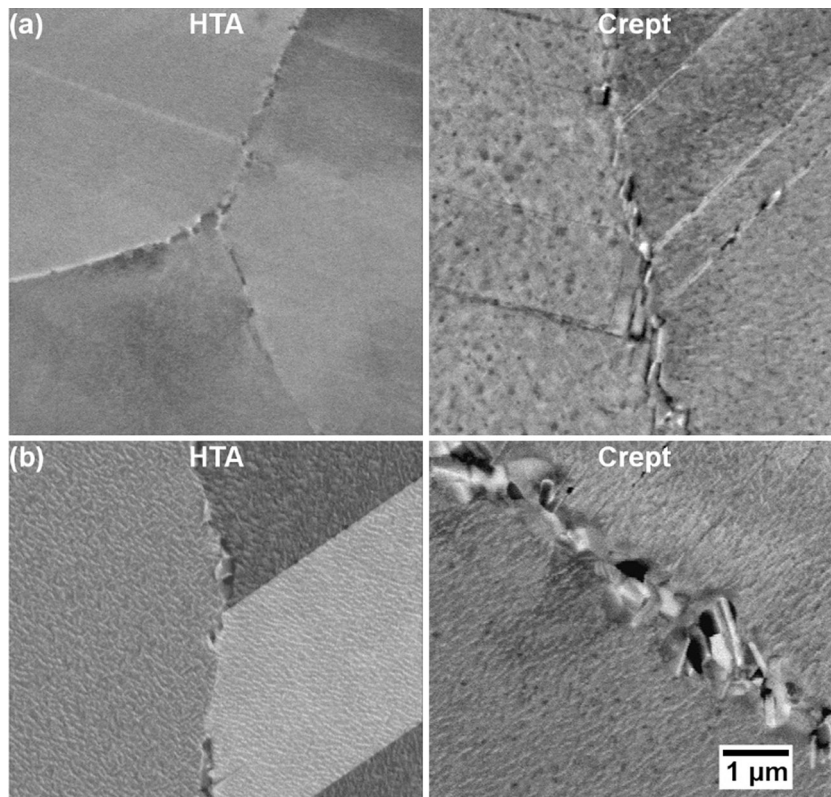


Fig. 6—SEM images comparing the HTA as-aged specimens and creep specimens in the gauge section following testing at 973 K (700 °C)/483 MPa for (a) alloy High(Ti/Al) and (b) Nb-High(Ti/Al), both in the HTA condition.

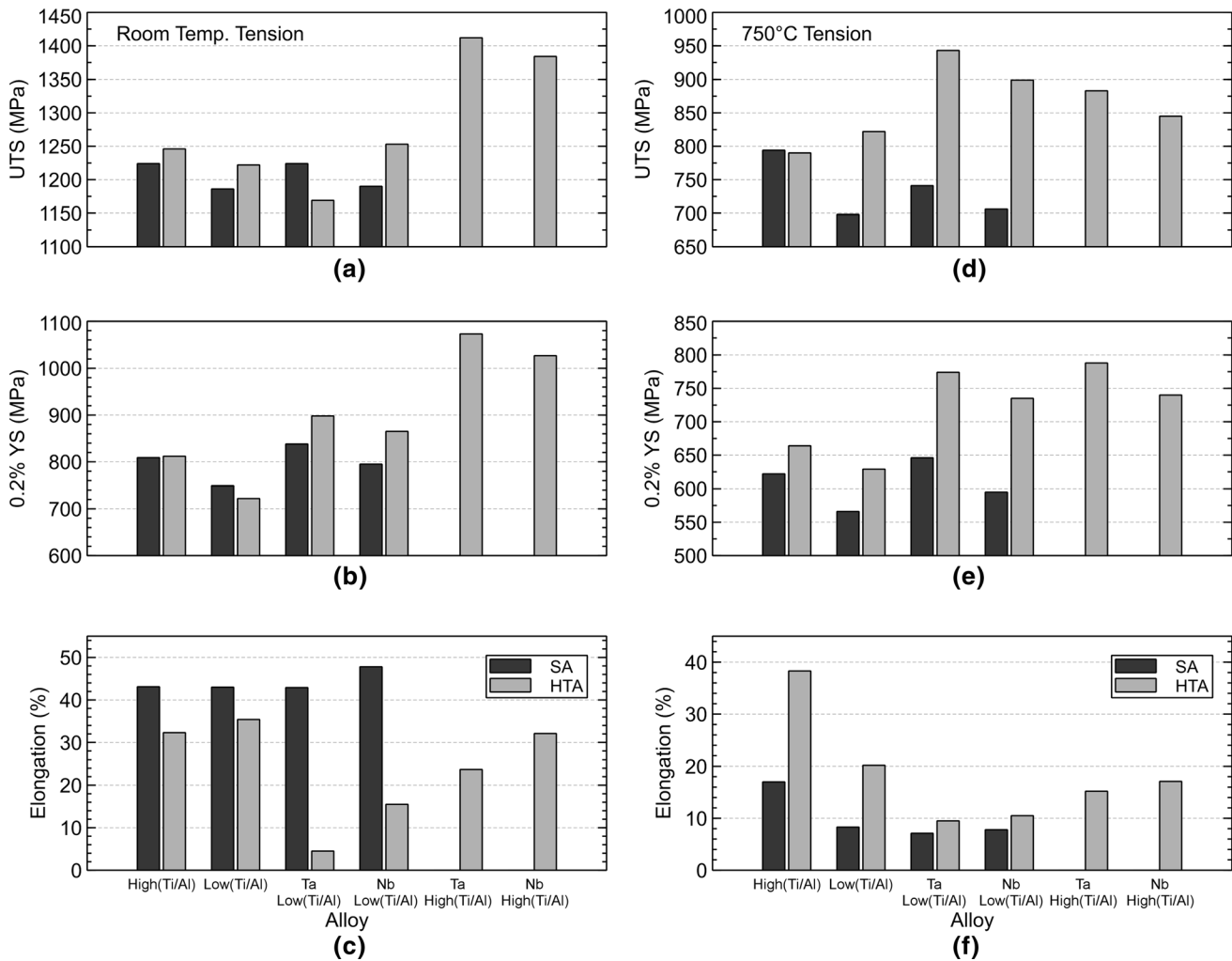


Fig. 7—Tension testing results at (a to c) room temperature and (d to f) 1023 K (750 °C) showing (a, d) UTS, (b, e) 0.2 pct YS and (c, f) elongation to failure for samples after standard aging (SA) and high temperature aging (HTA). Note: no data are shown for alloys Ta-High(Ti/Al) and Nb-Low(Ti/Al) after SA.

following the HTA heat treatment, particularly for alloys Ta-Low(Ti/Al) and Nb-Low(Ti/Al) (at 5 and 16 pct, respectively).

Testing at 1023 K (750 °C) revealed higher UTS and YS for alloys Ta-Low(Ti/Al), Nb-Low(Ti/Al), Ta-High(Ti/Al) and Nb-High(Ti/Al) following the HTA heat treatment compared to the other alloys/conditions, Figures 7(d) through (f). The values ranged from 845 to 943 MPa and 735 to 788 MPa for the UTS and YS, respectively. Lower values were measured for alloys High(Ti/Al) and Low(Ti/Al) as well as Ta-Low(Ti/Al) and Nb-Low(Ti/Al) in the SA condition. Most importantly, the UTS and YS were generally lower in the SA condition than in the HTA, as observed in Figures 7(d) and (e). The elongation to failure was reduced, particularly for the alloys following the SA heat treatment. For instance, alloys Low(Ti/Al), Ta-Low(Ti/Al) and Nb-Low(Ti/Al) presented elongations to failure around 8 pct. Values above 20 pct were measured for alloys High(Ti/Al) and Low(Ti/Al) in the HTA condition and above 10 pct for Nb-Low(Ti/Al),

Ta-High(Ti/Al) and Nb-High(Ti/Al) in the HTA condition.

IV. DISCUSSION

A. Effect of the HTA Heat Treatment

Differences in microstructures, tensile mechanical properties as well as creep performance were found between the SA and HTA heat treatments for a given alloy chemistry. Starting with the effect of the HTA on the microstructure, precipitation of the γ'' phase was more pronounced, as observed in Figure 3 when comparing Figures 3(g) and (a) and Figures 3(h) and 3(d) (see also the supplementary material). Note: While the images were taken from the creep specimens, the TEM samples were extracted from the grip which excluded the effect of strain. Furthermore, the time at the test temperature of 700 °C is not expected to significantly affect the aged microstructures since γ' and/or γ'' precipitates are already formed according to

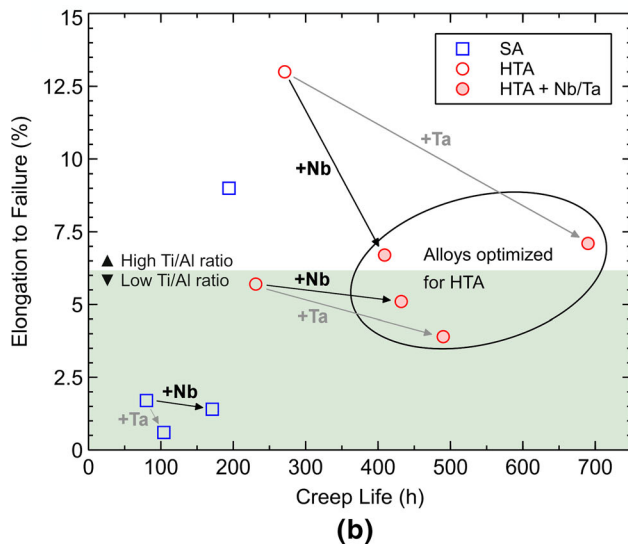
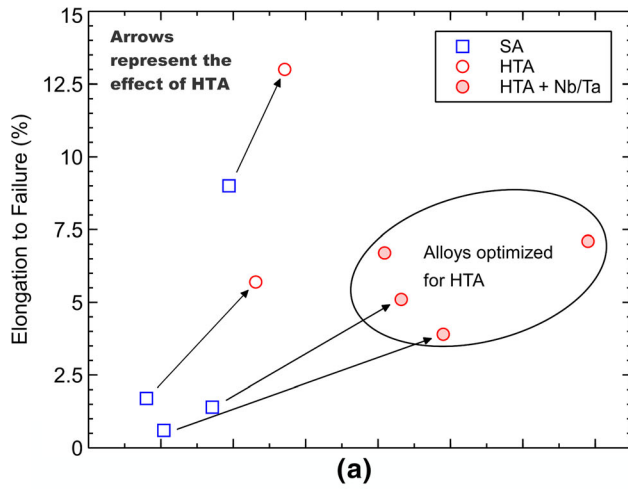


Fig. 8—Elongation to failure as a function of creep life at 973 K (700 °C) and 483 MPa illustrating the effects of (a) the HTA treatment and (b) the Nb and Ta additions.

Table V. Minimum Creep Rate (MCR) During Creep Testing at 973 K (700 °C)/ 483 MPa

Alloy	Aging	Minimum Creep Rate (Pct/h)
High(Ti/Al)	SA	0.0026
	HTA	0.0106
Ta-High(Ti/Al)	HTA	0.0012
Nb-High(Ti/Al)	HTA	0.0068
Low(Ti/Al)	SA	0.0045
	HTA	0.0053
Ta-Low(Ti/Al)	SA	0.0036
	HTA	0.0019
Nb-Low(Ti/Al)	SA	0.0030
	HTA	0.0011

the time-temperature-transformation (TTT) diagram of Mannan *et al.*^[10] and from inspection of the predicted TTT diagrams using JMatPro on the alloys of this

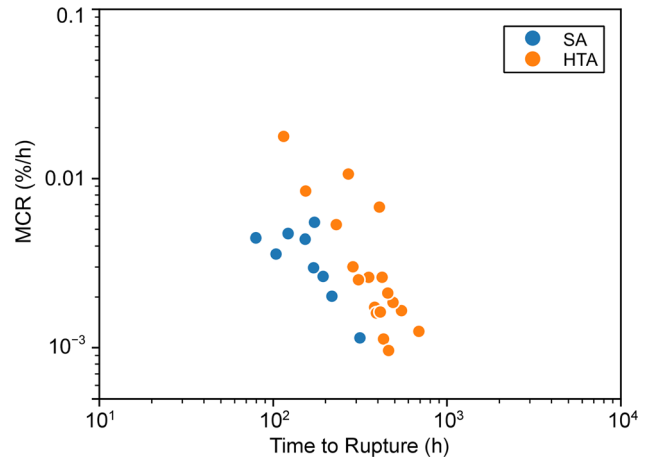


Fig. 9—MCR versus time to rupture for all test conditions and alloys with separation between the SA and HTA aging heat treatments.

investigation. Not only the precipitation of γ'' was promoted, coarsening of the precipitates was observed. Furthermore, the precipitation of secondary phases along the GBs, such as δ and/or η was promoted as well, as shown in Figure 2, while GB carbides appeared to have coarsened. The higher temperatures of the HTA treatment accelerated the kinetics of phase formation. In addition, the first step exposure time was higher at 1073 K (800 °C) and longer (20h) which enabled coarsening of the various precipitate phases compared to the SA heat treatment in which the first step consisted of 8h at 1003 K (730 °C).

As mentioned in the results section, Thermo-Calc simulations did not predict γ'' to form in the alloys. The γ'' phase is metastable, therefore, Thermo-Calc predicted its stable form which is δ phase. The $\gamma'' \rightarrow \delta$ transformation has been reported experimentally at elevated temperature, above 973 K (700 °C).^[30] This transformation was not observed in this investigation which is most likely related to the exposure time at temperature. Additional CALPHAD simulations were performed using JMatPro. The solvus temperature of the γ'' phase was predicted to be between 1093 K (820 °C) and 1133 K (860 °C) for these alloys. Note: Secondary precipitation along the GBs has been the subject of numerous investigations on IN718, particularly concerning the formation of δ phase. Typically, an additional step is used above the γ'' solvus temperature to promote the formation of δ precipitates.^[16] With the highest temperature in the HTA heat treatment being below the γ'' solvus temperature, it is not surprising to see little to no precipitation of δ phase (depending on the alloy) while γ'' precipitates were present in the microstructure, see Figure 3.

The effect of the HTA on the tensile properties was minimal at RT, with the exception of ductility which significantly decreased, particularly for alloys Ta-Low(Ti/Al) and Nb-Low(Ti/Al), as observed in Figure 7(c). At 1023 K (750 °C), however, significant increases in UTS and YS were measured when comparing SA and HTA conditions. The effect was stronger for

the alloys with higher levels of Nb and Ta, namely Ta-Low(Ti/Al) and Nb-Low(Ti/Al), Figures 7(d) and (e); the reason being attributed to the increased amount of γ'' precipitate strengthening in those alloys, Figure 3. Consequently, the HTA coupled with chemistry variations resulted in increases in UTS of up to 19 pct and YS of up to 27 pct at 1023 K (750 °C) from the standard alloy High(Ti/Al) SA. At RT, alloys Ta-High(Ti/Al) and Nb-High(Ti/Al) performed the best with increases in UTS and YS of up to 15 and 33 pct, respectively.

Figure 8 summarizes the effect of the various alloy design modifications on the creep performance at 973 K (700 °C) and 483 MPa. The effect of the HTA is illustrated in Figure 8(a). The HTA approach resulted in significant increases in both creep life and creep ductility, characterized by the elongation to failure, regardless of the alloy formulation. More precisely, the HTA resulted in the following improvements when compared to the SA: (i) a 40 pct increase in creep life and 53 pct increase in creep ductility for alloy High(Ti/Al), (ii) a 189 pct increase in creep life and 235 pct increase in

creep ductility for alloy Low(Ti/Al), (iii) a 371 pct increase in creep life and 550 pct increase in creep ductility for alloy Ta-Low(Ti/Al), and finally (iv) a 153 pct increase in creep life and 264 pct increase in creep ductility for alloy Nb-Low(Ti/Al). With the HTA promoting precipitation strengthening as well as precipitation at the GBs, additional obstacles to dislocation motion were created benefiting overall alloy creep capabilities. Furthermore, a denser repartition of the GB precipitates was formed during creep testing, as shown in Figure 6(b). These can provide further obstacles to grain boundary sliding and prevent cavity growth.^[31] The MCR was measured, and the results are reported in Table V. The HTA resulted in a decrease in MCR for the high Nb/Ta alloys, *i.e.*, Ta-Low(Ti/Al) and Nb-Low(Ti/Al), that showed the greatest improvements in creep life. However, the opposite was observed for the low Nb/Ta alloys High(Ti/Al) and Low(Ti/Al); therefore, the effect of the HTA on the MCR is not clear.

Creep testing under other conditions were investigated as presented in the results section for 1063 K (790 °C) and 207 MPa. However, the testing parameters 973 K (700 °C) and 483 MPa provided the most complete dataset for comparison of the SA and HTA heat treatments. Nevertheless, an overview of these alloy's creep performance is provided by plotting the MCR against the time to rupture in Figure 9. Both testing conditions are represented along with two additional ones, not shown in the results section, namely 998 K (725 °C)/414 MPa and 1023 K (750 °C)/345 MPa. From Figure 9, it is clear the HTA had a beneficial effect on the creep performance overall characterized by facilitating longer creep lives for equivalent MCRs. The results for the full list of tensile and creep testing conditions investigated are listed in the supplementary material.

B. Effect of the Nb and/or Ta Additions

To compare the effect of Nb and Ta additions it is important to remember the sum of both elements was nominally 2.7 at. pct in the high Nb/Ta alloys Ta-Low(Ti/Al), Nb-Low(Ti/Al), Ta-High(Ti/Al) and Nb-High(Ti/Al). The atomic mass for Ta being greater at approximately 181 u than that of Nb at approximately 93 u, the sum for both elements in wt pct, as listed in Table I for Nb and Ta, is not constant. Furthermore, the alloys were designed from the baseline of IN725 which contains Nb but no Ta. Therefore, adding Ta in alloys Ta-Low(Ti/Al) and Ta-High(Ti/Al) was in addition to the relatively high Nb level of 3.4 wt pct already present in the baseline alloy.

Focusing on creep testing at 973 K (700 °C) and 483 MPa, Figure 4(a), additions of Nb or Ta to alloy Low(Ti/Al) and similarly adding Nb or Ta to alloy High(Ti/Al) all resulted in increases in creep life. This observation is true regardless of the use of the HTA as summarized in Figure 8(b) where specimens are compared for each aging heat treatment and chemistry. It is important to note that the Nb and/or Ta additions were more effective at improving the creep properties of the

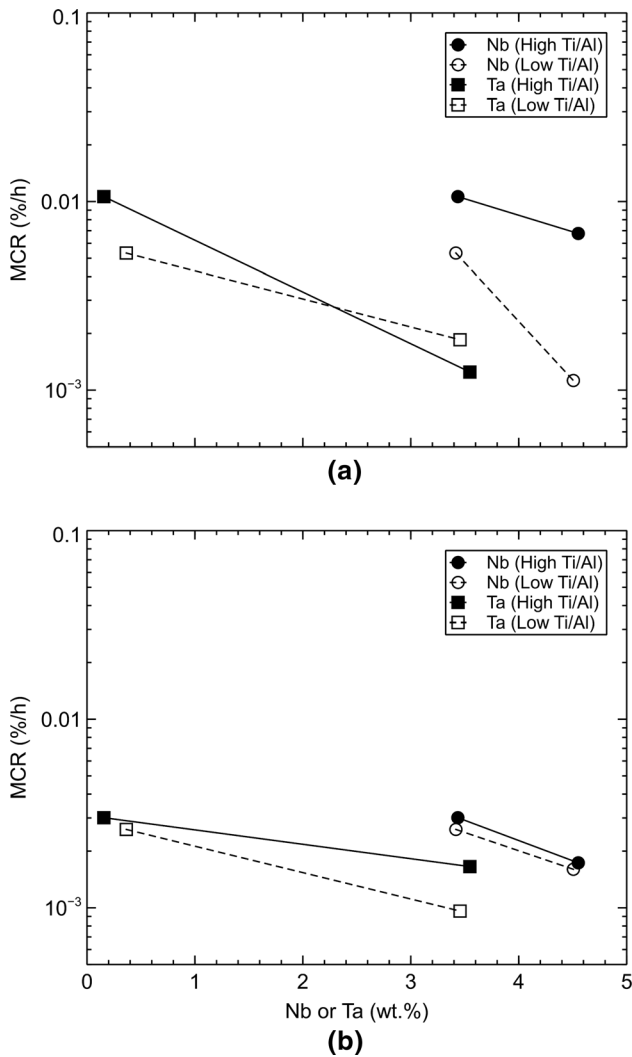


Fig. 10—MCR as a function of the Nb or Ta concentration for testing at (a) 973 K (700 °C) / 483 MPa and (b) 1063 K (790 °C) / 207 MPa.

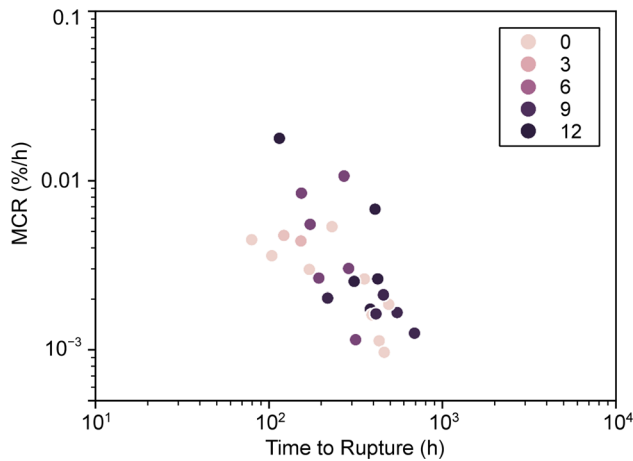


Fig. 11—Monkman-Grant relationship for all test conditions and alloys with coloring according to the Ti/Al ratio.

alloy when combined with the HTA heat treatment as shown in Figure 8(b) by comparing the effect of the addition for SA and HTA separately. From Figure 3, the additions increased the level of γ'' precipitate strengthening and, to a lesser extent, they also promoted the formation of GB phases such as δ precipitates, as observed in alloy Nb-Low(Ti/Al), Figure 2(f). In the low Ti/Al ratio alloys, the additions allowed for a compact morphology of the γ'/γ'' precipitates to form, as observed in Figures 3(e) and (f), while complete compacts were not obtained in alloy Low(Ti/Al), Figure 3(d).

Interestingly, the Thermo-Calc prediction showed Ta partitioning to the η phase in high-Ta alloys Ta-Low(Ti/Al) and Ta-High(Ti/Al), Table III, and increased η stability in the alloys aforementioned, Figure 1, which was not observed experimentally. Additional characterization and experimental data (such as long term exposure at temperature) will be needed to confirm. In a recent investigation, Ta has been reported to partition to the η phase and to be more effective at promoting η formation compared to Nb in high-Ta alloys.^[32] Other investigations have reported η chemistries consisting of Ni_6AlNb .^[20,33,34]

The influence of Nb and Ta were separated in Figure 10 by plotting the MCR as a function of the Nb or Ta concentration with results grouped by alloys of similar chemistry, *i.e.*, High(Ti/Al) vs Ta-High(Ti/Al), High(Ti/Al) vs Nb-High(Ti/Al), Low(Ti/Al) vs Ta-Low(Ti/Al) and Low(Ti/Al) vs Nb-Low(Ti/Al). Only the specimens that received the HTA heat treatment were considered. For all comparisons, adding Nb or Ta resulted in a decrease in MCR, thereby underlining the improved creep performance, primarily expressed as time to failure, of the high Nb/Ta alloys. This observation is valid for both testing conditions: 973 K (700 °C) and 483 MPa, Figure 10(a), and 1063 K (790 °C) and 207 MPa, Figure 10(b). The results of Figure 10, however, cannot be used to determine which addition was more beneficial to reducing the MCR. In other words, what balance of Nb and Ta in the Nb + Ta concentration was important, *i.e.*, the alloy almost

exclusively comprised Nb or the alloy comprised approximately of 1.7 at. pct Nb and 1.0 at. pct Ta. The reduced MCRs showed relatively close values when comparing both testing conditions and each addition, with the exception of the Nb (High Ti/Al) datapoint of Figure 10(a).

C. Effect of the Ti/Al Ratio

The Ti/Al ratio was decreased from >7 in the baseline alloy High(Ti/Al), and high Nb/Ta variants Ta-High(Ti/Al) and Nb-High(Ti/Al), to 1.3 in alloy Low(Ti/Al) and high Nb/Ta variants Ta-Low(Ti/Al) and Nb-Low(Ti/Al). This modification promoted the formation of γ' precipitates as opposed to γ'' which was confirmed in Figures 3(a) through (f). The γ' precipitates are often preferable for operation at high temperatures due to their greater solvus temperature compared to that of γ'' . However, the γ'' solvus temperature predicted using JMatPro fell between 1093 K (820 °C) and 1133 K (860 °C) depending on alloy chemistry. As such, testing was performed below the solvus temperatures of both precipitate phases. Furthermore, even the highest temperature in the HTA heat treatment was below the solvus temperature of the γ'' precipitates. Therefore, in addition to the γ' precipitates in the low Ti/Al ratio alloys, γ'' platelets formed on the facets of the γ' particles to create a compact morphology. Note: Although γ' precipitates were also present in some of the high Ti/Al ratio alloys, the significantly greater amount of γ'' precipitates compared to γ' did not allow for the formation of the compact structure.

The Ti/Al ratio also influenced the GB phases. In particular, for the high Ti/Al ratio alloys, the effect of adding Nb or Ta seemed to be concentrated within the grains (*i.e.*, an increase in the amount of γ'') with minimal effect at the GBs. In contrast, the effect of Nb/Ta additions on the low Ti/Al ratio alloys, seemed to be concentrated towards the GBs, particularly in alloy Nb-Low(Ti/Al), see Figure 2(f), and less so within the grain (characterized by the completion of compacts). With more γ' present in the low Ti/Al alloys, the Nb and Ta likely partitioned to the GB phases as opposed to γ'' in the high Ti/Al alloys. Nevertheless, avoiding δ phase formation at the GBs in a γ'' containing alloy may be preferable according to recent findings from Nicolay *et al.*^[35] on IN718. The authors showed improved mechanical properties by avoiding the first step of the three-step heat treatment, thereby reducing δ formation at the GBs and increasing the amount of γ'' precipitates within the grains, since the two phases have similar chemistries.

The effect of the Ti/Al ratio on the creep performance is less clear. While Figure 8(b) reveals that, for testing at 973 K (700 °C) and 483 MPa, high Ti/Al ratios led to elongations to failure greater than 6 pct and low Ti/Al ratios led to elongations to failure less than 6 pct this trend was not validated for testing at 1063 K (790 °C) and 207 MPa, Figure 4(b). This was further illustrated on the Monkman-Grant plot of Figure 11 which, like Figure 9, regroups additional testing conditions. From the results of Figure 11, however, a low Ti/Al ratio was

generally associated with shorter times to rupture for an equivalent MCR.

The alloys with the HTA heat treatment and Nb or Ta additions, regrouped in Figure 8 as “Alloys optimized for HTA” showed the greatest improvements in creep life for testing at 973 K (700 °C) and 483 MPa. Comparison to the baseline alloy High(Ti/Al) SA, condition most representative of IN725, reveals the following improvements in creep lives: (i) 111 pct with HTA and Nb addition, (ii) 123 pct with HTA, Nb addition and low Ti/Al ratio, (iii) 256 pct with HTA and Ta addition and (iv) 138 pct with HTA, Ta addition and low Ti/Al ratio.

V. CONCLUSIONS

Alloys with elevated levels of Nb and Ta were designed alongside a high temperature aging (HTA) heat treatment to promote the formation of desirable phases and improve the mechanical properties of a Ni-based superalloy. Based on the results and observations of this investigation, the following can be concluded:

1. The HTA promoted the formation and growth of γ'' precipitates as well as grain boundary phases, such as δ precipitates among others. This resulted in significant increases in time and elongation to failure for testing at 973 K (700 °C) and 483 MPa, and time to failure for testing at 1063 K (790 °C) and 207 MPa. Increases in UTS and YS were also measured at 1023 K (750 °C).
2. Similarly, additions of Nb and Ta had a positive effect on the creep performance, particularly on the time to failure. The additions were more beneficial when coupled with the HTA heat treatment. The MCR decreased similarly for both elemental additions, therefore, the balance of Nb and Ta in Nb + Ta = 2.7 at. pct did not significantly influence the creep behavior for the conditions investigated.
3. The Ti/Al ratio in the alloys with the HTA heat treatment controlled the predominant precipitation of γ' (low Ti/Al ratio of 1.3) or γ'' (high Ti/Al ratio >7) precipitates. For testing at 973 K (700 °C) and 483 MPa, a low Ti/Al ratio was associated with low creep ductility although this was not always valid for other testing conditions. A low Ti/Al ratio resulted overall in minor decreases in MCRs.
4. The effect of adding Nb or Ta in the alloys with the HTA heat treatment seemed to be concentrated within the grains (increase in the amount of γ'') with minimal effect at the GBs for the alloys with a high Ti/Al ratio. The opposite was observed in the low Ti/Al ratio alloys, in which the effect of Nb and Ta seemed to be more concentrated towards the GBs. With γ' present in the low Ti/Al alloys, the Nb and Ta likely partitioned to the GB phases as opposed to γ'' in the high Ti/Al alloys. However, adding Nb

and Ta to the low Ti/Al ratio alloys enhanced the precipitation of the γ'' precipitates leading to the formation of a compact morphology consisting of a γ'' shell surrounding the γ' precipitates.

5. The creep life of IN725 was improved by up to 256 pct for testing at 973 K (700 °C) and 483 MPa and by up to 73 pct for testing at 1063 K (790 °C) and 207 MPa using additions of Nb or Ta coupled with a higher temperature aging heat treatment.

ACKNOWLEDGMENTS

This work was performed in support of the US Department of Energy's Fossil Energy Crosscutting Technology Research Program. The authors would like to thank E.R. Argetsinger and J.A. Mendenhall for assistance in melting, C.D. Powell for mechanical testing, R.E. Chinn and C. McKaig for chemistry analysis and M.B. Fortner for metallographic preparation.

COMPETING INTEREST

The authors declare the following competing interests: authors M. Detrois, P.D. Jablonski and J.A. Hawk are inventors on a patent application assigned unto the United States Government on some of the presented alloy compositions and heat treatment. The present manuscript, however, describes the research and fundamental aspects related to microstructure—thermomechanical processing—mechanical property relationships.

DISCLAIMER

This project was funded by the United States Department of Energy, National Energy Technology Laboratory, in part, through a site support contract. Neither the United States Government nor any agency thereof, nor any of their employees, nor the support contractor, nor any of their employees, makes any warranty, express or implied, or assumes any legal liability or responsibility for the accuracy, completeness, or usefulness of any information, apparatus, product, or process disclosed, or represents that its use would not infringe privately owned rights. Reference herein to any specific commercial product, process, or service by trade name, trademark, manufacturer, or otherwise does not necessarily constitute or imply its endorsement, recommendation, or favoring by the United States Government or any agency thereof. The views and opinions of authors expressed herein do not necessarily state or reflect those of the United States Government or any agency thereof.

SUPPLEMENTARY INFORMATION

The online version contains supplementary material available at <https://doi.org/10.1007/s11661-022-06690-6>.

REFERENCES

1. R. Viswanathan, J.F. Henry, J. Tanzosh, G. Stanko, J. Shingledecker, B. Vitalis, and R. Purgert: *J. Mater. Eng. Perform.*, 2005, vol. 14, pp. 281–92.
2. F. Abe: *Engineering*, 2015, vol. 1, pp. 211–24.
3. M. Fukuda, Y. Yagi, H. Fukutomi, S. Nishinoiri, K. Sato, T. Nishii, K. Nishimaki, T. Takano, H. Aoki, Y. Okuma, T. Furukawa, M. Shimada, N. Saito, K. Hashimoto, M. Kitamura, E. Saito, H. Semba, Y. Matsubara, K. Takahashi, T. Takahashi, and T. Suga: in *Joint EPRI-123HiMAT International Conference on Advances in High Temperature Materials*, J. Shingledecker and M. Takeyama, eds., ASM International, Nagasaki, Japan, 2019, pp. 1487–99.
4. H. Hack, R. Purgert, and R. Schrecengost: in *Joint EPRI-123HiMAT International Conference on Advances in High Temperature Materials*, J. Shingledecker and M. Takeyama, eds., ASM International, Nagasaki, Japan, 2019, pp. 1476–86.
5. K. Kubushiro, K. Nomura, T. Matsuoka, H. Nakagawa, and K. Muroki: *IHI Eng. Rev.*, 2016, vol. 49, pp. 34–43.
6. R. Purgert, J. Phillips, H. Hendrix, J. Shingledecker, and J. Tanzosh: 2016, p. 79.
7. M.C. Hardy, M. Detrois, E.T. McDevitt, C. Argyrakis, V. Saraf, P.D. Jablonski, J.A. Hawk, R.C. Buckingham, H.S. Kitaguchi, and S. Tin: *Metall. Mater. Trans. A.*, 2020, vol. 51, pp. 2626–50.
8. Special Metals Corporation: *INCONEL Alloy 725*, 2005.
9. L.E. Shoemaker: *6th Int. Symp. Superalloys 718, 625, 706 Deriv.*, 2005, pp. 409–18.
10. S. Mannan and F. Veltry: in *Superalloys 718, 625, 706 and Various Derivatives*, E.A. Loria, ed., TMS (The Minerals, Metals & Materials Society), 2001, pp. 345–56.
11. S.K. Mannan, E.L. Hibner, and B.C. Puckett: *Corrosion*, 2003, p. 3125.
12. M. Detrois, P.D. Jablonski, and J.A. Hawk: *Mater. Sci. Eng. A*, 2021, vol. 799, p. 140337.
13. E.L. Hibner, H.W. Sizak, and S.K. Mannan: *Superalloys 718, 625, 716 Deriv.*, 1997, pp. 491–501.
14. M. Detrois, K.A. Rozman, P.D. Jablonski, and J.A. Hawk: in *Proceedings of the 9th International Symposium on Superalloy 718 & Derivatives: Energy, Aerospace, and Industrial Applications*, E. Ott, X. Liu, J. Andersson, Z. Bi, K. Bockenstedt, I. Dempster, J. Groh, K. Heck, P.D. Jablonski, M. Kaplan, D. Nagahama, and C. Sudbrack, eds., Springer International Publishing, Pittsburgh, PA, 2018, pp. 421–37.
15. A. Agnoli, M. Bernacki, R. Logé, J.M. Franchet, J. Laigo, and N. Bozzolo: in *Superalloys 2012: 12th International Symposium on Superalloys*, E.S. Huron, R.C. Reed, M.C. Hardy, M.J. Mills, R.E. Montero, P.D. Portella, and J. Telesman, eds., TMS (The Minerals, Metals & Materials Society), 2012, pp. 73–82.
16. H.-Y. Bor, C.-N. Wei, H.T. Nguyen, A.-C. Yeh, and C.-M. Kuo: in *7th International Symposium on Superalloy 718 and Derivatives*, E.A. Ott, J.R. Groh, A. Banik, I. Dempster, T.P. Gabb, R. Helmink, X. Liu, A. Mitchell, G.P. Sjöberg, and A. Wusatowska-Srnek, eds., TMS (The Minerals, Metals & Materials Society), 2010, pp. 679–88.
17. L. Viskari, Y. Cao, M. Norell, G. Sjöberg, and K. Stiller: *Mater. Sci. Eng. A.*, 2011, vol. 528, pp. 2570–80.
18. E.J. Pickering, H. Mathur, A. Bhowmik, O.M.D.M. Messé, J.S. Barnard, M.C. Hardy, R. Krakow, K. Loehnert, H.J. Stone, and C.M.F. Rae: *Acta Mater.*, 2012, vol. 60, pp. 2757–69.
19. M. Detrois, S. Antonov, R.C. Helmink, and S. Tin: *Jom.*, 2014, vol. 66, pp. 2478–85.
20. S. Antonov, M. Detrois, R.C. Helmink, and S. Tin: *J. Alloys Compd.*, 2015, vol. 626, pp. 76–86.
21. P.D. Jablonski and J.A. Hawk: *J. Mater. Eng. Perform.*, 2017, vol. 26, pp. 4–13.
22. ASTM International: *ASTM E8/E8M-16a, Standard Test Methods for Tension Testing of Metallic Materials*, West Conshohocken, PA, 2016.
23. ASTM International: *ASTM E139-11(2018), Standard Test Methods for Conducting Creep, Creep-Rupture, and Stress-Rupture Tests of Metallic Materials*, West Conshohocken, PA, 2018.
24. K.A. Rozman, M. Detrois, T. Liu, M.C. Gao, P.D. Jablonski, and J.A. Hawk: *J. Mater. Eng. Perform.*, 2020, vol. 29, pp. 5822–39.
25. Z. Xu, L. Jiang, J. Dong, Z. Li, and X. Zhou: *J. Alloys Compd.*, 2015, vol. 620, pp. 197–203.
26. R. Cozar and A. Pineau: *Metall. Trans.*, 1973, vol. 4, pp. 47–59.
27. R. Cozar and A. Pineau: *Metall. Trans.*, 1974, vol. 5, pp. 2471–2.
28. J. He, G. Han, S. Fukuyama, and K. Yokogawa: *Acta Mater.*, 1998, vol. 46, pp. 215–23.
29. ASTM International: *ASTM E112-13, Standard Test Methods for Determining Average Grain Size*, West Conshohocken, PA, 2013.
30. L.M. Suave, J. Cormier, P. Villechaise, A. Soula, Z. Hervier, D. Bertheau, and J. Laigo: *Metall. Mater. Trans. A.*, 2014, vol. 45A, pp. 2963–82.
31. M. Detrois, P.D. Jablonski, and J.A. Hawk: in *Superalloys 2020*, S. Tin, ed., Springer International Publishing, Seven Springs, PA, 2020, pp. 171–81.
32. L. Finet, V.A. Esin, V. Maurel, and L. Nazé: in *Superalloys 2020*, S. Tin, ed., Springer, Cham, 2020, pp. 112–21.
33. M. Rath, M. Rath, E. Povoden-Karadeniz, and E. Kozeschnik: *Superalloys.*, 2016, vol. 2016, pp. 97–105.
34. X. Xie, G. Wang, J. Dong, C. Xu, W.-D. Cao, and R. Kennedy: *Superalloys 718, 625, 706 Var. Deriv.*, 2005, pp. 179–91.
35. A. Nicolaÿ, J. Franchet, N. Bozzolo, and J. Cormier: in *Superalloys 2020*, Tin S. et al., ed., Springer, Cham, 2020, pp. 559–69.

Publisher's Note Springer Nature remains neutral with regard to jurisdictional claims in published maps and institutional affiliations.